CFD Modeling
of a Small Hydro Kaplan Turbine

Reilly Smith

Undergraduate Honors Thesis

April 2021

Mechanical Engineering

Advisor: Dr. Clarissa Belloni

Abstract

Although hydropower is already a significant contributor to energy generation in the US, there are still ways for it to expand. One of these ways is to enable existing small, low-head dams and weirs to generate energy through Kaplan-style turbines. This project develops a 3D Computational Fluid Dynamics (CFD) model of Rickly Hydro's 92L32 PROPEL, Kaplan-style Turbine to optimize performance in low-head applications. This CFD model will help to save time and cost for the optimization of the turbine's geometry and operation. The flow through the turbine is simulated using ANSYS Fluent under various operating conditions to provide results over the turbine's entire operating space. The main set of simulations look at the transient effects of the turbine blades rotating at different speeds. Torque and other flow field data values are presented. These results are then compared to experimental and field results obtained from the manufacturer to validate the CFD model. Multiple simulations are conducted to predict the performance under different operating conditions. Future work for this project will involve manipulating the geometry of the turbine to optimize its performance based off the operating conditions given. Specifically, propeller and wicket gate angles can be adjusted to optimize performance under certain flow rates.

Acknowledgements

I would like to thank Dr. Belloni for the opportunity to be a part of her research group. She has provided useful support and advice throughout the entirety of my project. She is the reason this project was possible and I am very thankful for her support.

I would also like to give a big thank you to Ryan Cook and the whole Rickly team. They gave me the opportunity to do this project on their turbine and have provided me with all the information I have needed over the course of this project.

I also owe a thank you to Rodrigo Auza Gutierrez for his guidance throughout the project. His expertise and advice on CFD was a huge reference for me.

I would like to thank the rest of the SIMCenter team, especially Amber Pasternak, for helping with whenever I had issues with the OSC. I would also like to thank them for the access to the computing resources needed to complete this project.

Table of Contents

List of Figures

List of Tables

Nomenclature

Acronyms:

CFD: Computational Fluid Dynamics
EGL: Energy Grade Line
EIA: Energy Information Administration
OSC: Ohio Supercomputer
URANS: Unsteady Reynolds Averaged Navier Stokes

Symbols:

C_f: Skin Friction Coefficient
C_L: Characteristic Length
C_m: Moment Coefficient
g: Gravitational Constant
H_{net}: Net Head
$\eta_{turbine}$: Efficiency of Turbine
P: Power
P: Pressure
ρ: Density
Q: Flow Rate
T: Torque
U_∞: Free Stream Velocity
μ: Dynamic Viscosity
V: Flow Velocity
ω: Rotational Speed
y_p: Distance to Wall Adjacent Cell Center

1. Introduction

1.1 Low Head Hydropower

Renewable energy, specifically hydropower, is a rapidly growing and evolving field. While the installation of civil structures, such as dams and weirs which hydropower depends on, have slowed down due to environmental issues, there are still many ways to grow the hydropower field. Hydropower already produces a generous portion of energy in the US. In fact, in 2019 hydropower produced 274 kWh or 6.6% of energy in the US. (EIA 2019) However, a study performed by the Department of Energy's Oak Ridge National Laboratory found that the US still has 12 GW of potential energy available in non-powered dams. (Energy.gov 2014) Figure 1.1 shows the locations of these non-powered dams in the US.

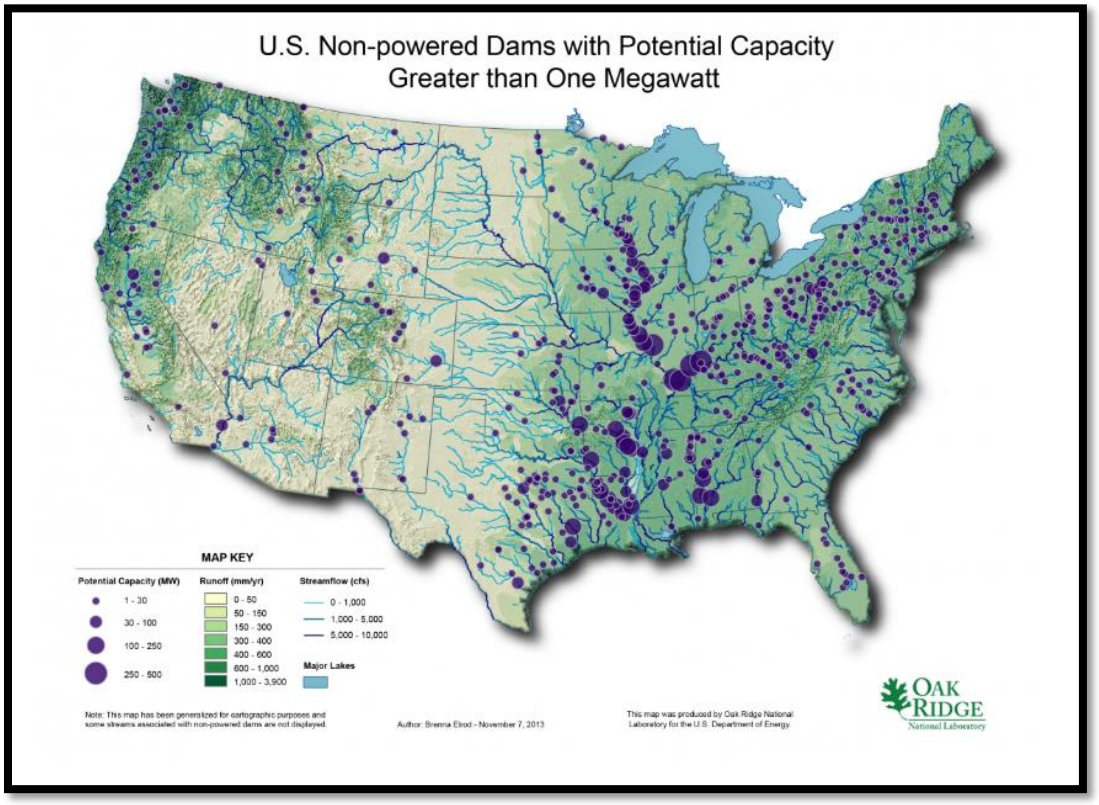

Figure 1.1: Non-Powered Dams in the United States (Energy.gov 2014)

A large share of these non-powered dams are small hydropower locations. Small hydropower plants are typically defined as plants that generate between 1-10 MW. (Breeze 2018) Small hydropower non-powered dams are represented in Figure 1.1 by the smallest symbol. According to World Bank in 2018, small hydropower made up 7% of the hydropower energy produced in the US. (Breeze 2018) However, there is still a lot of room to grow. In 2016, the International Center on Small Hydropower estimated the global capacity for small hydropower was 78,000 MW. (Breeze 2018)

One of the more promising ways to grow the field of small hydropower is by powering low head dams. Low head hydropower plants produce energy with a head of less than 30 m. (Breeze 2018)

However, because of the limited power able to be generated by these low head sites, upfront construction costs can cause the installation of these plants to be economically unjustified. Because of this many companies have tried to get creative with how to utilize these low head sites without requiring a large construction cost.

One company working to solve this issue is Rickly Hydropower based out of Columbus, OH. One of their creative ways to utilize non-powered low head dams is called their PROPEL-Hydro System. In this system, water is siphoned over the dam and passed through a Kaplan style turbine to generate power. A picture demonstrating this system can be seen in Figure 1.2.

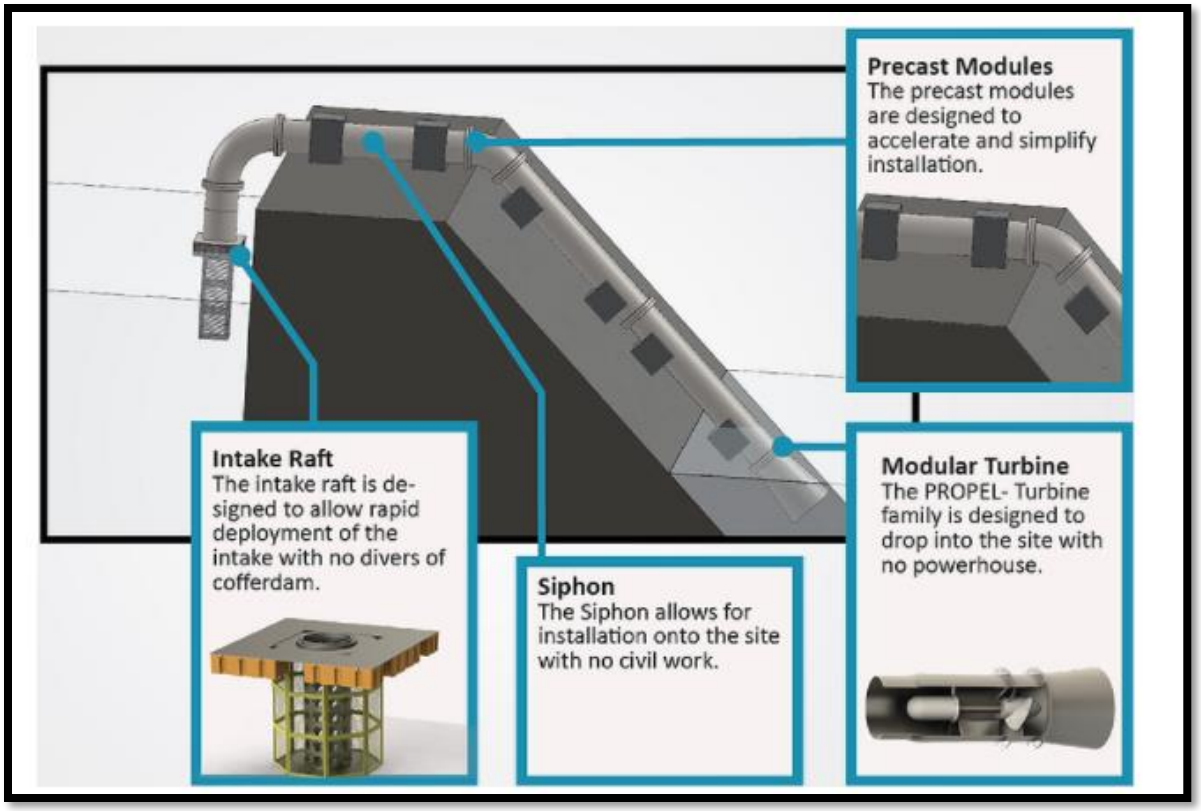

Figure 1.2: Rickly's PROPEL-Hydro System (Rickly 2020)

1.2 Low Head Hydropower Turbines

To generate energy from these non-powered low head sites multiple different types of turbines have been utilized. One of the most commonly used turbines for low head application are Kaplan turbines. Kaplan turbines, developed by Viktor Kaplan in 1915, are propeller type, axial turbines with adjustable blades. They are very similar to propeller turbines in both their application and functionality. The main difference is that propeller turbines are single regulated since they only control flow rate with the wicket gates. Kaplan turbines are double regulated meaning that the flow rate can adjusted through changing the pitch on the runner blades. Rickly Hydropower has a Kaplan-style turbine called the PROPEL Turbine, which can be seen in Figure 1.3.

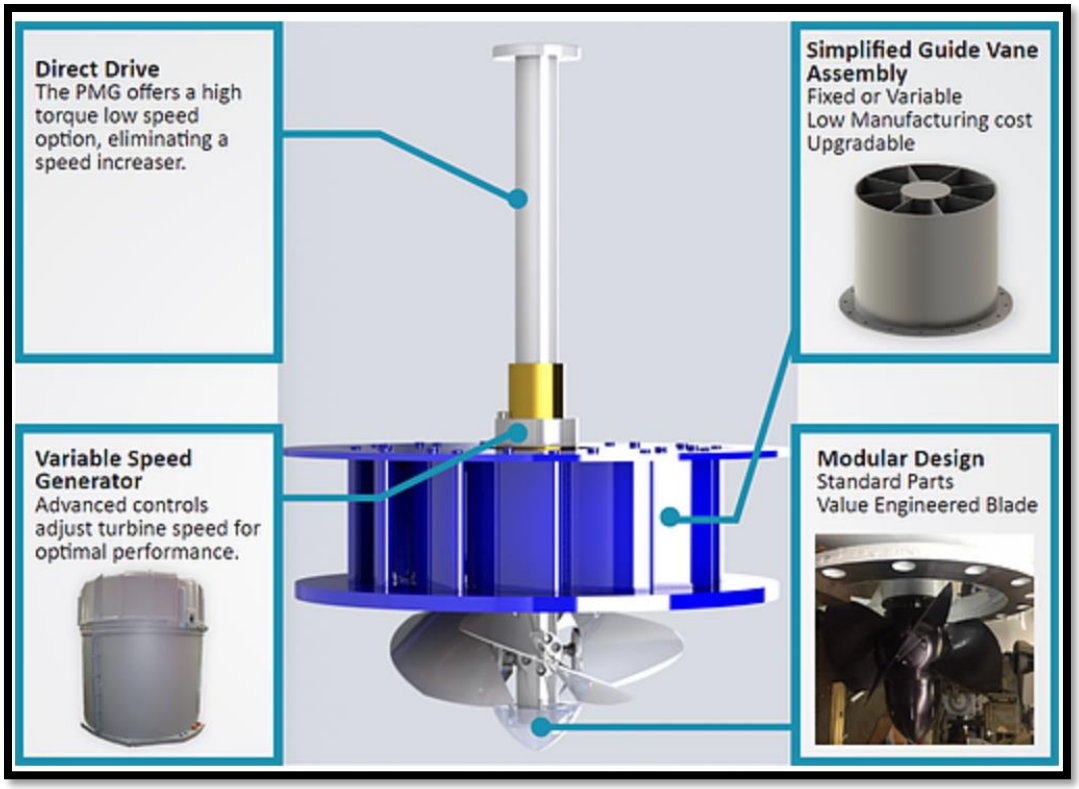

Figure 1.3: Rickly's PROPEL Turbine (Rickly 2020)

As discussed previously, Kaplan turbines are double regulated. The PROPEL turbine has adjustable wicket gates located at the inlet to control flow rate. The PROPEL turbine's rotor blade angles can also be adjusted for optimal performance.

This turbine has 7 different sizes of varying diameters: 18 in, 28 in, 32 in, 40 in, 48 in, 60 in, and 72 in. Each of these different turbines has a different operating range. A chart showing each turbine's accepted operating heads and discharges can be seen in Figure 1.4. The 32-inch version of the PROPEL turbine, which is used in this project, is not pictured on this chart. However, it can be assumed that a portion of the 32-inch version's operating range will be within the operating range of both the 28- and 40-inch versions.

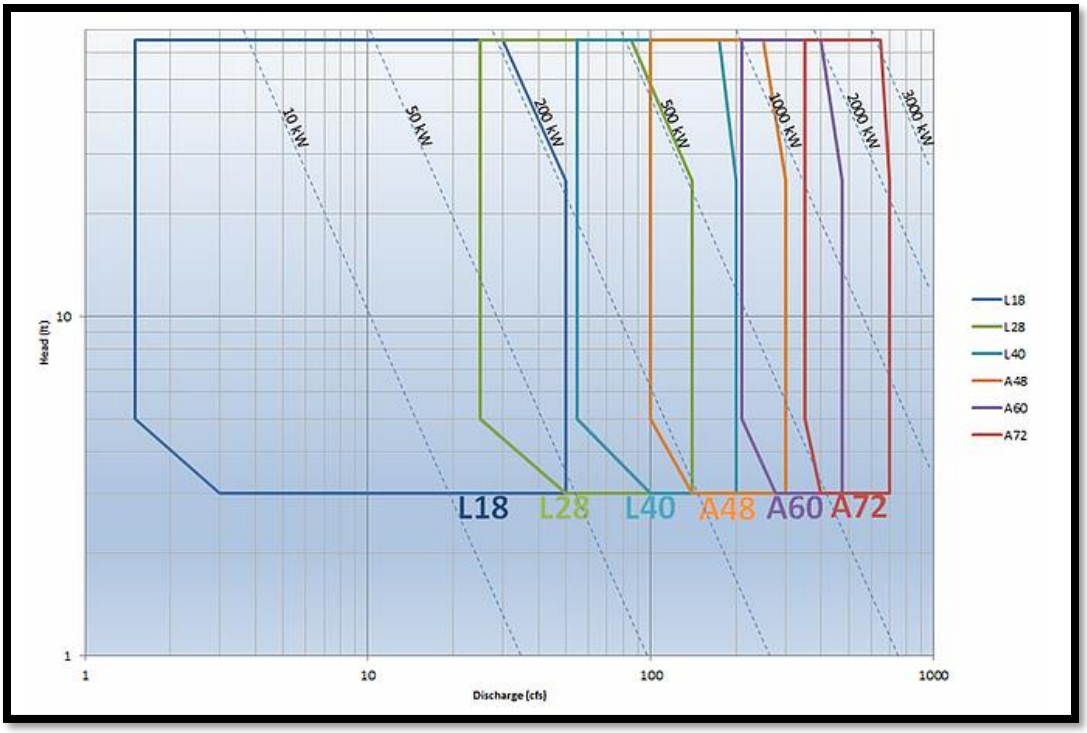

Figure 1.4: Chart of the Operating Ranges of Rickly's PROPEL Turbines (Rickly 2020)

A table showing the estimated power and operating conditions for Rickly's PROPEL turbines can also be seen in Table 1.

Table 1: Estimated Power and Operating Ranges of Rickly's PROPEL Turbines (Rickly 2020)

Model	Power (kW)	Flow (cfs.)	Head (ft.)	Propeller OD (in.)
PROPEL92L18	0.5-200	1.5-50	3-65	18
PROPEL92L28	50-500	25-140	3-65	28
PROPEL92L40	100-800	55-200	65	40
PROPEL92A48	200-1150	100-300	65	48
PROPEL92A60	300-1850	210-475	65	60
PROPEL92A72	500-3000	350-700	65	72

1.3 Thesis Objectives

For every operating condition a turbine experiences, there is an optimal combination for the wicket gate and propeller angles of the turbine to provide the highest efficiency performance possible. Experimentally finding this optimal geometry can be very time intensive. To solve this issue, this thesis will develop a CFD model of Rickly's 92L32 PROPEL turbine to provide a quicker and cheaper path to the future geometry optimization of this turbine. To validate that this simulation is accurate, it will be compared and validated against experimental data collected by Rickly from the PROPEL turbine at actual power sites.

To summarize the main objectives of this study are to:

- Develop a CFD Model of Rickly's PROPEL Turbine
- Validate the numerical Model using Experimental Data
- Future Work: Manipulate Geometry to Optimize Turbine Performance

1.4 Literature Review

Before conducting this thesis, literature was studied for reference and knowledge when starting the project. Specifically, other research publications regarding CFD simulation, especially on Kaplan turbines, were found and analyzed.

A previous study of a PROPEL turbine was performed by Rickly in 2017 (Cook 2017). In this study a pressure inlet was used in combination with a flow bound outlet. Because these boundary conditions were used on a very similar turbine as the one in this thesis, this is where the initial boundary conditions used in this study derived from. This study found that torque was able to be predicted within 2% accuracy of previous studies on the turbine. It also found the torque was very sensitive to the angle of attack of the runner.

Multiple other papers including a 2011 CFD study of a tubular Kaplan turbine by Vishal Soni and Kiran Patel were found to have used a velocity inlet and pressure outlet (Soni, Patel 2011). The tubular Kaplan turbine means that instead of a spiral casing inlet the turbine uses a straight convergent inlet. This study looked to validate their CFD model based off experimental results from turbines currently installed in China. They concluded that their simulation was accurate and that the CFD model could be used in early design stages for optimization.

Another paper found using these boundary conditions was a vertical Kaplan turbine CFD study by the same authors (Soni, Patel 2012). These authors did the same test as before where they verified their CFD model based of test results. They also were able to conclude that their CFD model was accurate and could be used to optimize the turbine's performance. This study tested at multiple different operating points to validate further the model's accuracy.

Another paper that was found was a 2020 study done by Yunzhe Li and Qilini Liu of a CFD study of a Kaplan turbine (Li, Liu 2020). In this study the authors tested different design variations to see what geometrical design led to optimal performance. The authors tested different inlets and different numbers of blades. In this study, the authors used the SST k-omega turbulence model and used a mass flow inlet in combination with a pressure outlet. The authors concluded that the hydraulic loss in the spiral case inlet in less than in the guide vane or draft tube. They also concluded that the number of blades determines the optimal discharge for the turbine.

2. Hydropower Systems

2.1 Analyzing Hydropower Systems

When analyzing hydropower systems, we typically evaluate the power produced by a plant compared to the theoretically available power. To calculate the theoretical maximum power available to the turbine, P_{max}, the pressure head available to the turbine, H, can be multiplied with the volumetric flow rate, Q, passing through the turbine.

$$P_{max} = H \times Q \tag{2.1}$$

The head, H, in this equation is typically given as the net head, H_{net}, though sometimes the gross head, H_{gross}, is also employed. Both are defined in figure 2.1. The gross head is the total pressure head between the upstream and downstream reservoir. Since the surface of each reservoir is at atmospheric pressure and the velocity can be approximated to zero at the surface, this results in a simple difference in heights, as shown in Equation 2.3. The net head is the total pressure head between the inlet to the turbine and the exit of the draft tube. Therefore, the net head will be smaller than the gross head. Equation 2.2 shows the expression for the net head:

$$H_{net} = \left(\frac{p_B}{\rho g} + \frac{{V_B}^2}{2g} + z_B\right) - \left(\frac{p_D}{\rho g} + \frac{{V_D}^2}{2g} + z_D\right) \tag{2.2}$$

And equation 2.3 the definition of the gross head:

$$H_{gross} = z_A - z_E \tag{2.3}$$

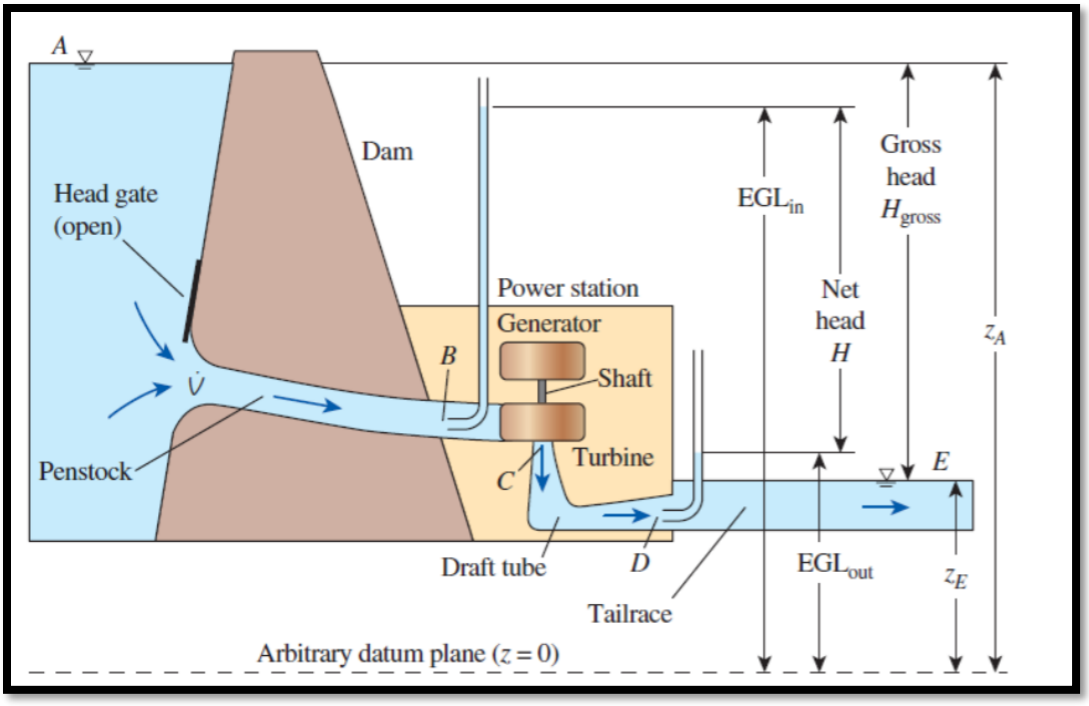

Figure 2.1: Schematic Demonstrating Net Head (Cengel)

The efficiency of the turbine can then be calculated by dividing the measured or simulated power by the theoretical maximum power. This can be seen in equation 2.4.

$$\eta_{turbine} = \frac{P_{sim}}{P_{max}} \tag{2.4}$$

2.2 Rickly Hydro's PROPEL Turbine

The diagram of the geometry of Rickly's 92L32 PROPEL Turbine can be seen Figure 2.2:

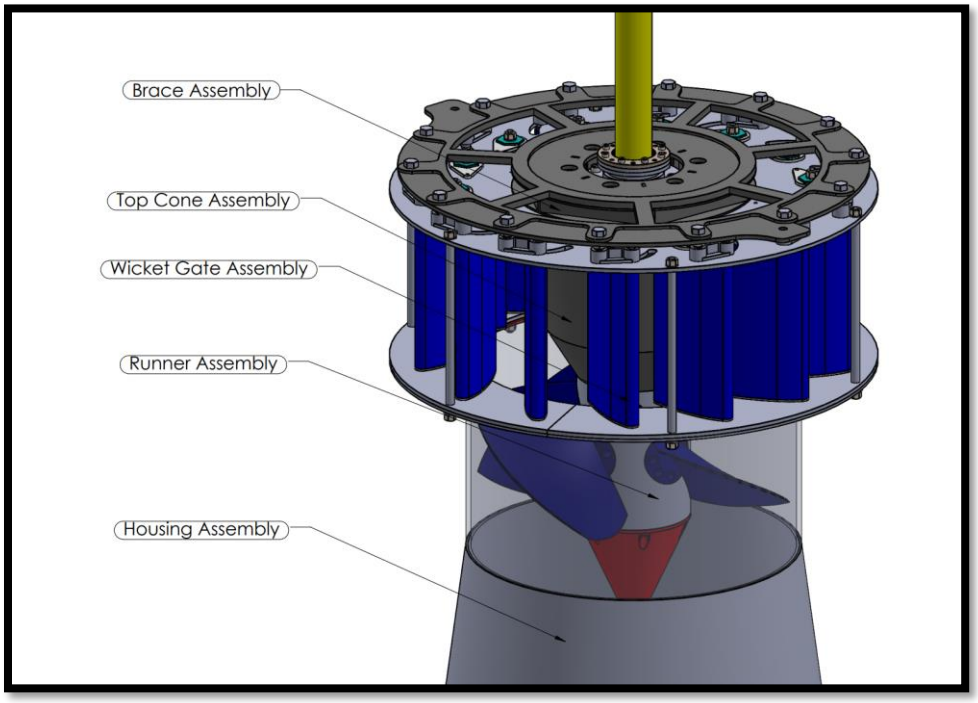

Figure 2.2: SolidWorks Geometry of the 92L32 PROPEL Turbine (Rickly 2020)

As can be seen, the water enters through the wicket gates. The angle of these wicket gates can be adjusted by the bracket assembly at the very top. The water then hits the top cone assembly, which directs water downwards towards the propellers. The propellers spin the shaft which is attached to a generator for energy generation. As mentioned previously the angle of the blades can also be adjusted for optimal performance.

For the 32-inch version of the PROPEL turbine, water is fed through the wicket gates by using a pressure box. The pressure box, which can be seen within Figure 2.3, uniformly pressurizes the water to a specific pressure (based on the upstream available head) before it passes through the wicket gates. This allows for the inlet conditions to be uniform leading to optimal performance.

The SolidWorks model of the PROPEL turbine in Figure 2.3 pictures half of the pressure box. The pressure box usually would be twice as tall with water entering the chamber through a valve halfway up on of the sides.

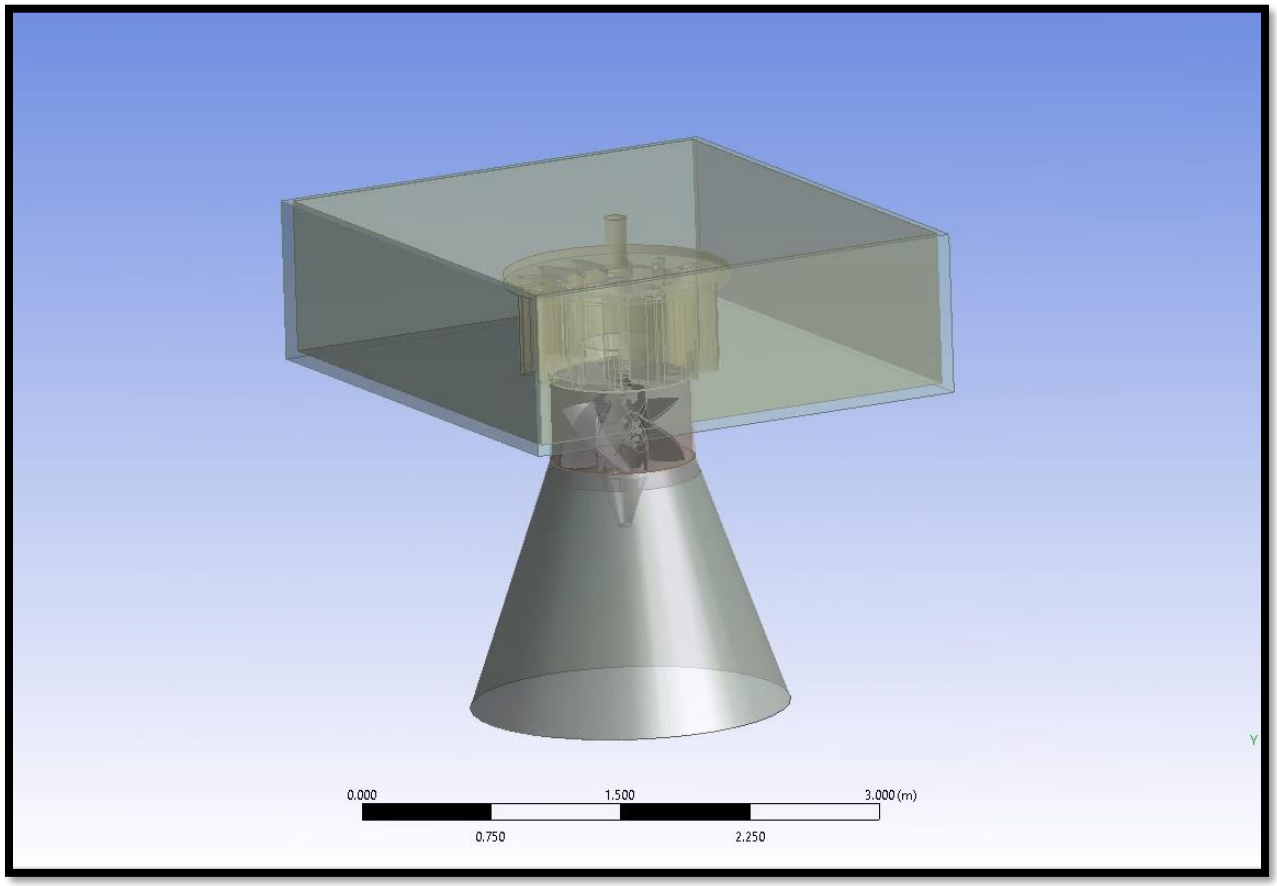

Figure 2.3: SolidWorks Model of 92L32 PROPEL Turbine Including Pressure Box

3. Computational Methods

3.1 Governing Equations

In this project, the Reynolds Averaged Navier Stokes equations were primarily used in unsteady form. The URANS equations consist of the continuity and momentum equation which can be seen below in equations 3.1 and 3.2.

$$\text{Continuity: } \frac{\partial u_i}{\partial t} + \frac{\partial u_i}{\partial x_i} = 0 \tag{3.1}$$

$$\text{Momentum: } \rho \frac{\partial \overline{u}_i}{\partial t} + \rho u_j \frac{\partial \overline{u}_i}{\partial x_j} = -\frac{\partial p}{\partial x_i} + \frac{\partial}{\partial x_j}\left[\mu \left(\frac{\partial \overline{u}_i}{\partial x_i} + \frac{\partial \overline{u}_i}{\partial x_j}\right) - \overline{\rho u'_\iota u'_j}\right] \tag{3.2}$$

The turbulence model chosen for this project was chosen to be the SST k-omega model. This was chosen due to it being the best model for turbomachinery and internal flows (Soni, Patel 2011). If future work were to be done using this CFD model, the turbulence model could be switched to check if there is a significant change.

3.2 Geometry

The turbine parts in SolidWorks format were obtained by Rickly for use in this study. Before creating a turbine assembly, the turbine parts needed to be simplified for use within CFD, since complexity needs to be reduced to achieve a reasonable meshing effort. In this process, any element of a part which had a negligible effect on the flow of water through the turbine was removed to make the meshing process easier, which would in turn allow for a decrease in computing time once simulations were run. An example of a part that was simplified was the

wicket gate assembly which can be seen in Figure 3.1. The pitch angle chosen for this project was 29 degrees while the wicket gates were set to 100% open at 63.127 degrees.

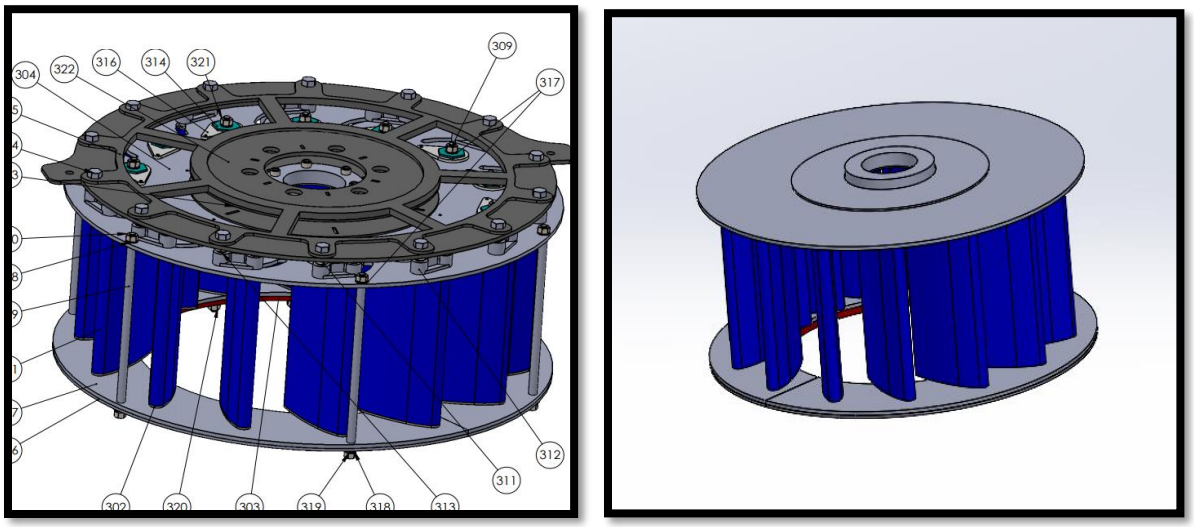

Figure 3.1: Wicket Gate Simplification

As shown the brace assembly was removed since its effect on the flow through the wicket gates was deemed insignificant. Using the same rationale, the poles for wicket gate adjustment were also deemed negligible in the CFD study. Both of these changes simplified the meshing process significantly and allowed for a fewer number of elements and therefore less computing time. Simplifications like these were made to all parts within the final assembly.

Once the assembly was created within SolidWorks, it was imported into Design Modeler for final preparation before meshing. The inlet was assigned to be at the top of the pressure box and the outlet was specified at the end of the draft tube. Three domains were created within the turbine: upper, inner, and lower. The upper included mostly the pressure box and the entrance of fluid through the wicket gates. The inner domain featured the blades and hub. The lower domain consisted of the fluid exiting the turbine through the draft tube. Figure 3.2 details the finished geometry, including the raised inlet.

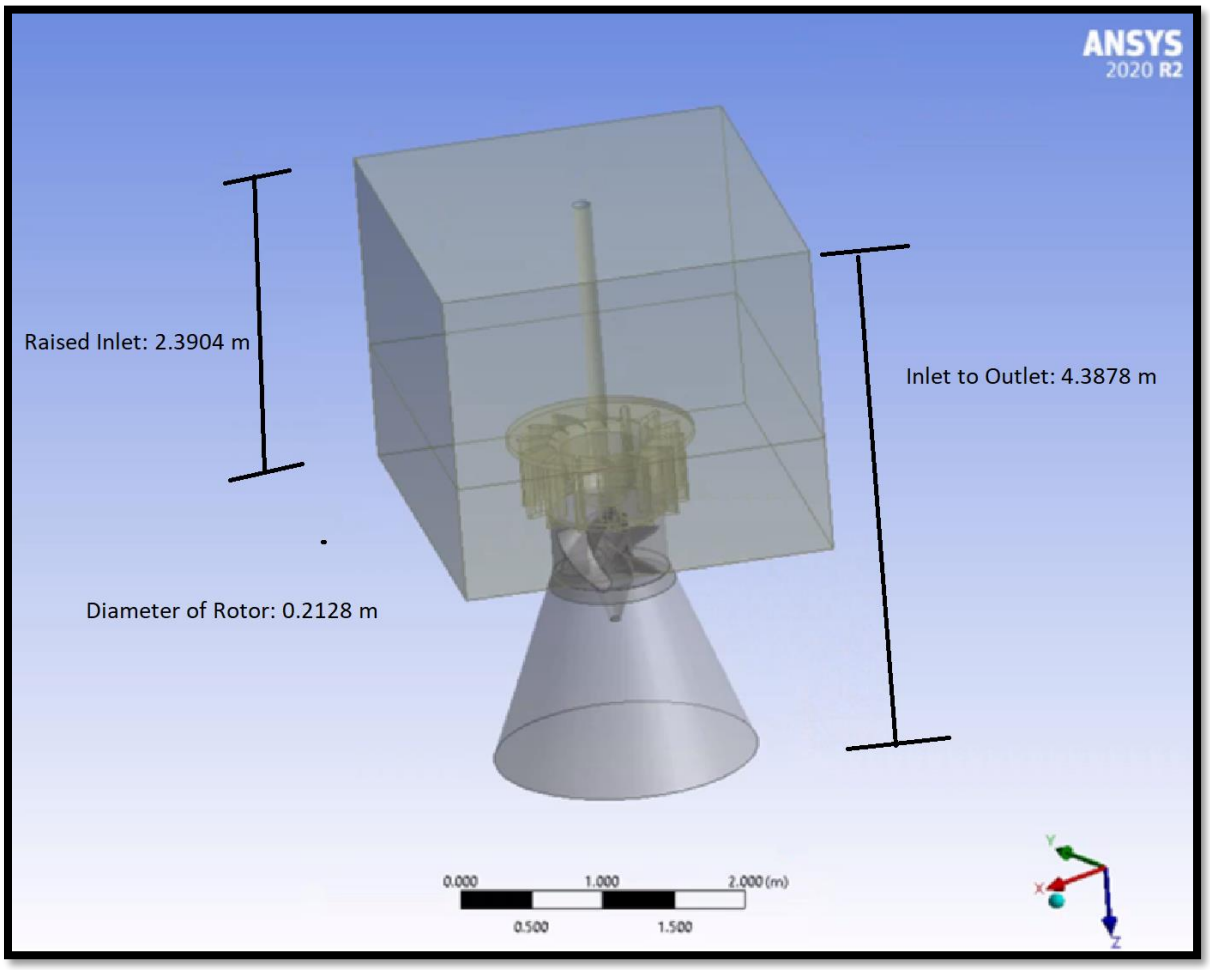

Figure 3.2: Finished Design Modeler Geometry

3.3 Mesh

For this project, an unstructured mesh was used. The converged mesh consisted of 4,824,850 elements and 1,430,128 nodes. The maximum element size in the flow domain was set to 0.3 m. The mesh was separated into three different domains which were the same as specified in the geometry. A picture of the final mesh can be seen in Figure 3.3.

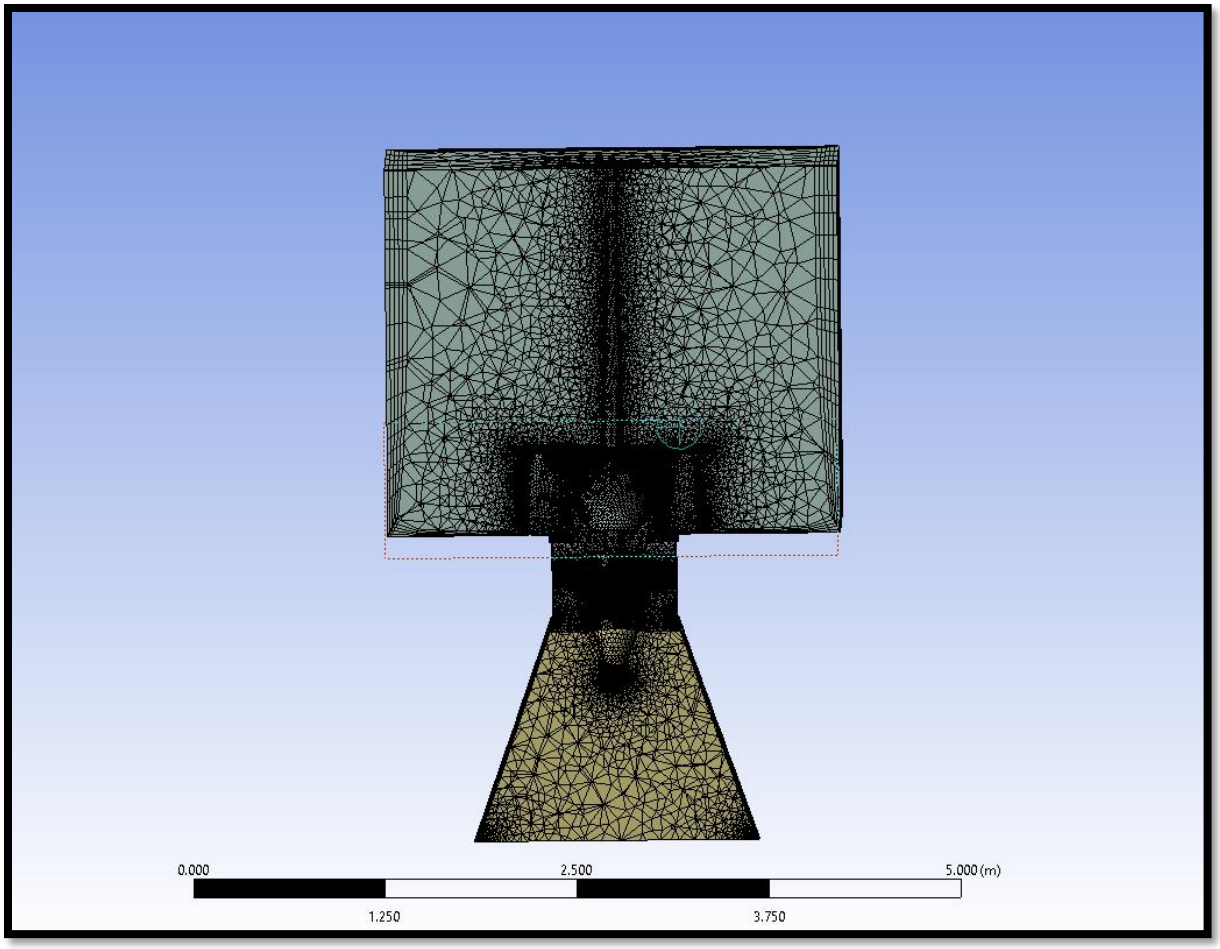

Figure 3.3: Picture of Final Mesh

As can be seen in the picture above, the elements in the mesh are biased towards areas of importance. These areas of importance include all walls especially within the wicket gates and inner domain.

To bias the cells towards these areas of importance, inflation layers were used. Inflation layers make sure that the boundary layer of all surfaces is covered with small enough elements. On all surfaces, between 5-8 layers were used. The inflation layers were specified using the first layer thickness and used a growth rate of between 1.0 and 1.4. A table showing all surfaces, their first layer height, number of layers, and growth rate can be seen in Table 2.

Table 2: Inflation Layer Statistics

Surface(s)	Number of Layers	First Layer Thickness (m)	Growth Rate
Top Cone	5	3.00E-03	1.05
Top Plate Shaft (top)	5	3.00E-03	1.05
Bottom of Pressure Box	5	3.00E-03	1.4
Walls of Pressure Box	5	3.00E-02	1.0
Hub Bottom Cone	6	3.07E-04	1.4
Blades	5	3.18E-04	1.25
Walls of Inner Domain	7	3.00E-04	1.4
Draft Tube Walls	5	3.00E-03	1.25
Wicket Gates	5	3.00E-03	1.05
Shaft (in Inner Domain)	8	3.07E-04	1.4
Shaft (in Upper Domain)	5	3.07E-04	1.4

To calculate the first layer thickness for the inflation layers on the blade surfaces, multiple equations were combined. The first equation can be seen below in equation 3.3.

$$y^+ = \frac{y_p \mu_t}{\nu} \tag{3.3}$$

This equation calculates the y+ value, which was chosen to be 10. The variable y_p is what was used as the first layer thickness for the inflation layers. The variable μ_t can be calculated using equation 3.4.

$$\mu_t \approx U_\infty \sqrt{\frac{C_f}{2}} \tag{3.4}$$

In equation 3.4, U_∞ is the free stream velocity c_f is the skin friction coefficient. The skin friction coefficient can be calculated by using equation 3.5 below. The free stream velocity in this study was 6.85 m/s (22.47 ft/s).

$$\frac{C_f}{2} \cong \frac{0.032}{Re^{\frac{1}{4}}} \tag{3.5}$$

Re in the equation above stands for Reynolds number which was calculated to be 1.96 x 10^6. This value was calculate using equation 3.6 below. The values used were taken from the inner domain. The speed was 6.85 m/s

$$Re = \frac{\rho V L}{\mu} \tag{3.6}$$

Based off these equations, the first layer thickness for the blades was found to be 3.18 x 10^{-4} m (10.43 x 10^{-4} ft).

A picture of the inflation layers on the blade surfaces can be seen in Figure 3.4.

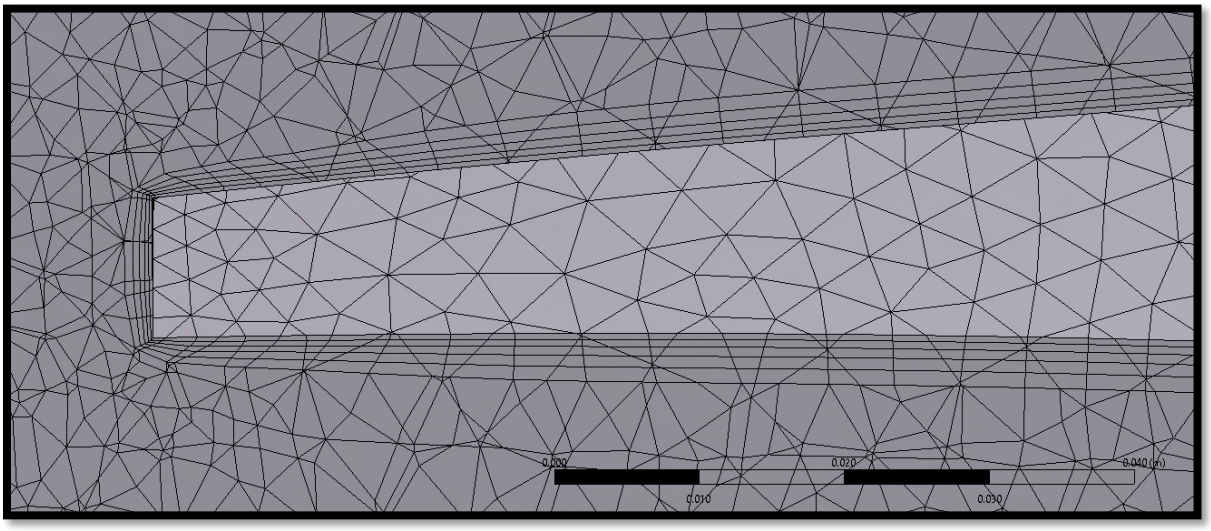

Figure 3.4: Inflation Layers on Blades

For all other surfaces, scaled first layer thicknesses were used based off the surface's importance to the flow of the water.

To make sure the mesh was refined enough near the blade, a face sizing was added to the blades' surfaces. The maximum size for elements on the blades' surfaces was set to 0.005 m. A picture of the face sizing on the blades can be seen in Figure 3.4.

3.4 Boundary Conditions

Multiple boundary conditions pairings were considered for the inlet and outlet. These boundary conditions were based on literature review.

The pairings tested were:

- Pressure Inlet and Mass Flow Outlet
- Velocity Inlet and Pressure Outlet

The first simulation trials were performed using a pressure inlet and a mass flow outlet. The gage pressure in the pressure box was chosen according to the data provided by the manufacturer of 88.942 Pa (12.9 psi). The flow rate at the outlet was specified as 1.982 m^3/s (70 cfs). Since the simulation trials using these boundary conditions failed to converge due to reversed flow through the inlet, this approach was abandoned.

The boundary condition combination employed in subsequent simulations was that of velocity inlet with pressure outlet. The velocity was specified at 0.21829 m/s at the inlet. This value was calculated by choosing a flow rate within the turbine's operating range of 1.699 m^3 / s (60 cfs)

and then dividing it by the area of the inlet which was 7.771 m^2 (83.65 ft^2). This can be seen in equation 3.7 below where Q is the flow rate, V is the velocity, and A is area.

$$Q = VA \tag{3.7}$$

The pressure outlet was set to 0 gage pressure. Figure 3.5 illustrates the location of the inlet and outlet. All walls in this simulation were set as no slip.

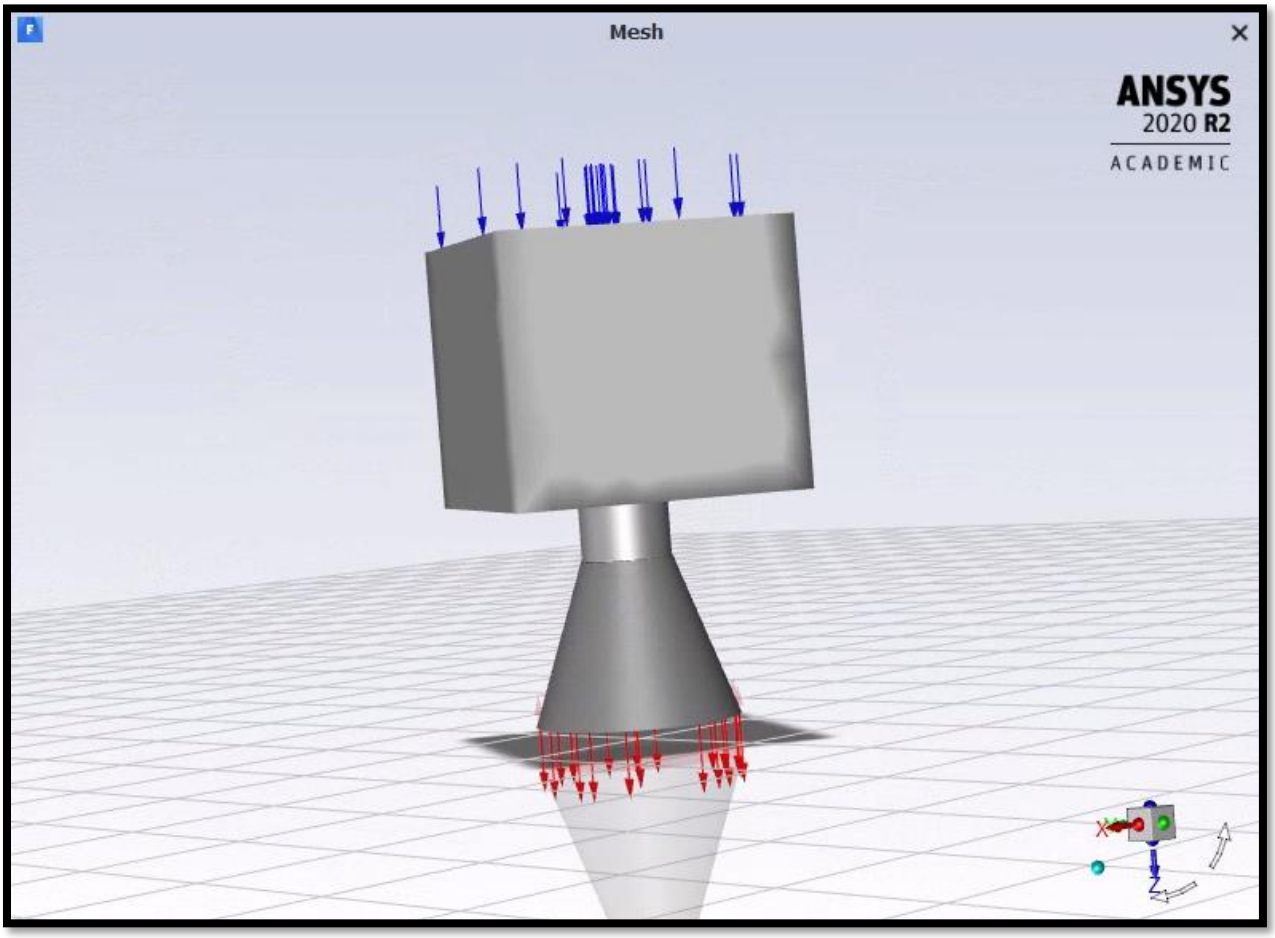

Figure 3.5: Inlet and Outlet Locations

For this simulation, gravity was assumed to be negligible due to the short vertical distance of the turbine. Thus, gravity was disabled in the simulation.

To simulate the rotation of the blades, a moving mesh was used. This was implemented in the inner domain where the propellers and hub are placed. The rotational speed was set as 32.46 rad/s (310 rpm) for the original case. Further cases of 27.591 rad/s (263.5 rpm), 37.329 rad/s (356.5 rpm), 42.198 rad/s (403 rpm), and 58.129 rad/s (555 rpm) were also simulated.

Because this simulation was transient, a calculated number of time steps and time step size were used to obtain a specific number of full rotations of the propellers. Simulations were run for 10,000 time steps for the rotational speed of 32.46 rad/s (310 rpm). The time step size chosen was 0.0003870967742 seconds. These values correspond to the rotor of the turbine turning a full 20 rotations. This also corresponds to a flow time of 3.87 seconds. The flow time of the fluid through the turbine was approximated to be around 0.63 seconds from inlet to the outlet. This estimate was found by calculating the flow speeds at different points throughout the turbine and the distance traveled by the fluid.

Table 3 shows the rotational speeds simulated and the number of rotations the rotor turned for each.

Table 3: Rotational Speeds and Number of Rotations

Rotational Speed (rad/s)	Full Rotations
27.591 (263.5 rpm)	17
32.46 (310 rpm)	20
37.329 (356.5 rpm)	23
42.198 (403 rpm)	26
58.129 (555 rpm)	36

Throughout the simulations run in this thesis, torque was monitored. To do this, a moment monitor was defined within the simulation to output the moment coefficient. This means that at each time step during the simulation a moment calculation (C_m) was obtained by from analyzing the surfaces of all four blades. From this coefficient, a torque value, T, could be obtained through using equation 3.8 below. The velocity (V) used in the calculation was from the inner domain where the rotor is located and was 6.85 m/s (22.47 ft/s). C_L is defined as the characteristic length. In this scenario the characteristic length was taken to be the diameter of the rotor.

$$T = 0.5 \times C_m \times C_L \times \rho \times V^2 \tag{3.8}$$

From this torque value, the shaft power, P_{sim}, can be calculated using equation 3.9 below where T is torque and ω is the rotational speed in rad/s.

$$P_{sim} = T \times \omega \tag{3.9}$$

To calculate the efficiency, the available head must be calculated. Based on the extent of the domain modeled, the net head (see Equation 2.2 in chapter 2) can be directly obtained by subtracting total pressure at the outlet from the total pressure at the inlet of the simulation domain. Note that gravity was turned off for this simulation and hence the elevation head component in Equation 2.2 was zero.

3.5 Ohio Supercomputer

Because the simulation is three-dimensional, has a large number of elements, and has a moving mesh, the computing power needed to run this simulation is greater than a normal computer can handle. To solve this issue, the Ohio Supercomputer was used to run these simulations. As a student at Ohio State apart of a research group, access to the supercomputer was granted through the OSU SimCenter. For each run on the supercomputer, case and data files were written from ANSYS Fluent with specific settings for each run. A journal and script file were then created. Examples of these files can be seen in Appendix A. The simulations used 14 nodes on the supercomputer and were set for a maximum run time of 60 hours. This run time was set as more time than needed to ensure the simulation ran its full course.

4. Results and Discussion

4.1 Convergence

4.1.1 Grid Convergence

To ensure that the computationally most efficient mesh was employed, a grid convergence study was performed. To perform this, the mesh was unrefined to consist of a smaller number of

elements, hence a coarser mesh. The number of elements tested was around half of the original mesh. The exact number of elements was 2,543,850.

After generating a mesh with a reduced number of cells, a simulation was performed employing the same settings at a rotational velocity of 42.198 rad/s. The simulation diverged which may be an indication that the original finer mesh was required. Due to time constraints on the Ohio Supercomputer, it was not possible to complete a finer mesh simulation by the deadline for the thesis completion. Therefore, full grid convergence has not been proven for the presented results.

To achieve full grid independence multiple more simulations must be run. First another simulation with the coarser mesh must be performed. The mesh could be manipulated to check if it will converge under different inflation layer and face sizing settings.

Another simulation with a finer mesh must also be run. If the results match the current results obtained, then it shows that the current mesh is good enough and that refining the mesh is unnecessary. If the results change, however, this shows that the mesh needed to be refined for accurate results.

Grid refinement is also necessary at the transition from the inner domain to the lower domain. The elements in the inner domain are much more refined than the elements in the lower domain. A smoother transition between element sizes between these two domains is necessary for a fully refined mesh.

4.1.2 Simulation Convergence

After the first simulation was run at 32.46 rad/s it was noticed that as the simulation progressed the moment coefficient converged successfully to a specific value. This trend can be seen in

Figure 4.1, which shows the torque plotted against the flow time in the simulation. As seen in Figure 4.1, the flow converges after around 2 seconds. This showed that the simulation time could be reduced to save time. Future simulations were able to be run for a shorter time of 6,000 times steps due to this convergence.

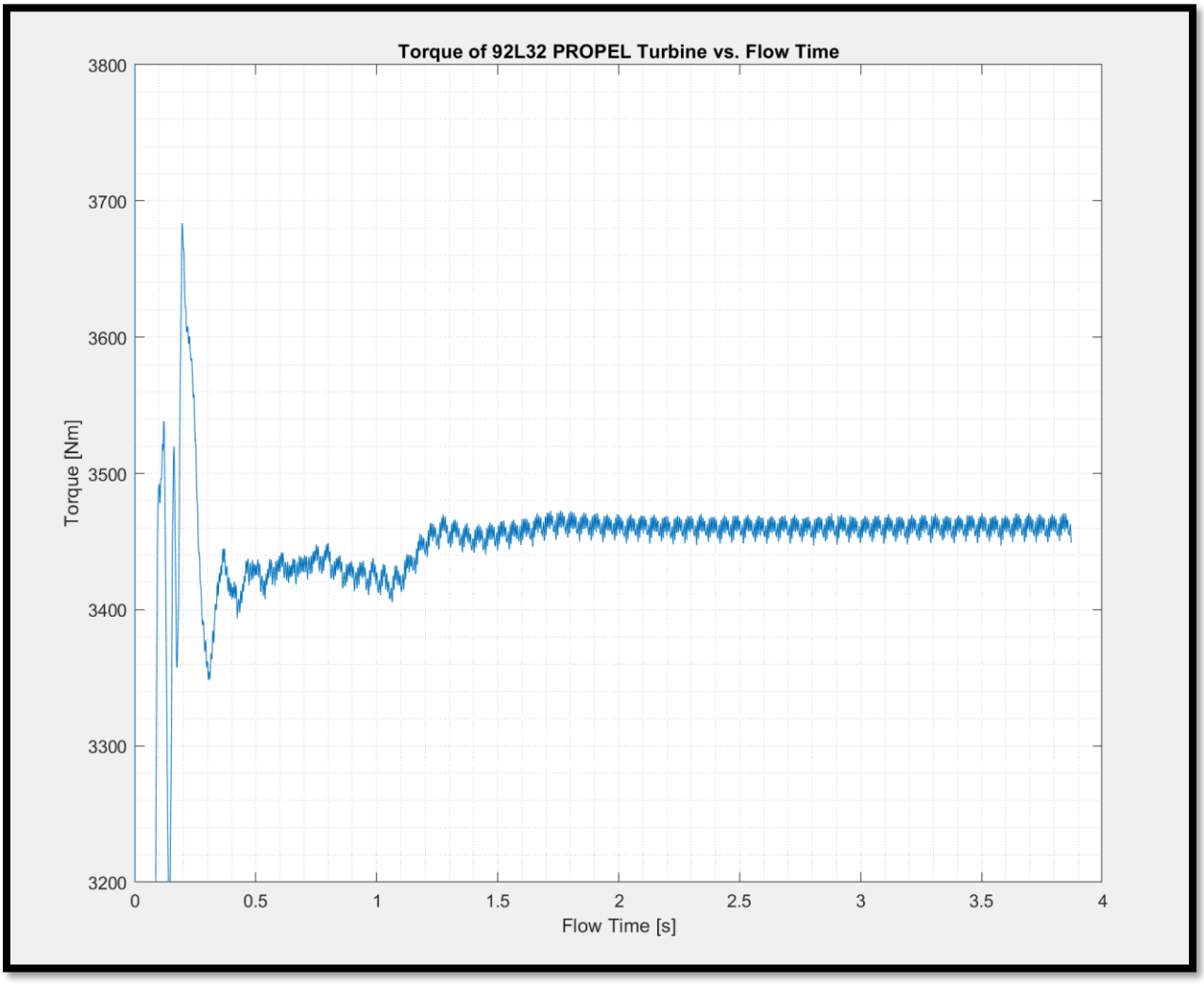

Figure 4.1: Plot of Torque vs. Flow Time for 32.46 rad/s

4.2 Flow Field Results

The following four rotational velocities were tested:

- 27.591 rad/s (263.5 rpm)
- 32.46 rad/s (310 rpm)
- 37.329 rad/s (356.5 rpm)
- 42.198 rad/s (403 rpm)
- 58.129 rad/s (555 rpm)

The first simulation was run for 10,000 timesteps. A plot of the residuals met the convergence criteria of 1×10^{-3}. Continuity had the largest residuals which fluctuated between 1×10^{-2} and just below 1×10^{-3}. As stated earlier, the simulations were able to be reduced to 6,000 timesteps due to the torque convergence.

The intention of running multiple rotational velocities was to explore a range of operating conditions. The flow field is analyzed using contour plots of pressure and velocity, presented here.

A graphic of the pressure contours throughout the turbine can be seen in Figure 4.2. As expected, we observe a significant pressure drop across the turbine associated with the energy extracted by the rotor.

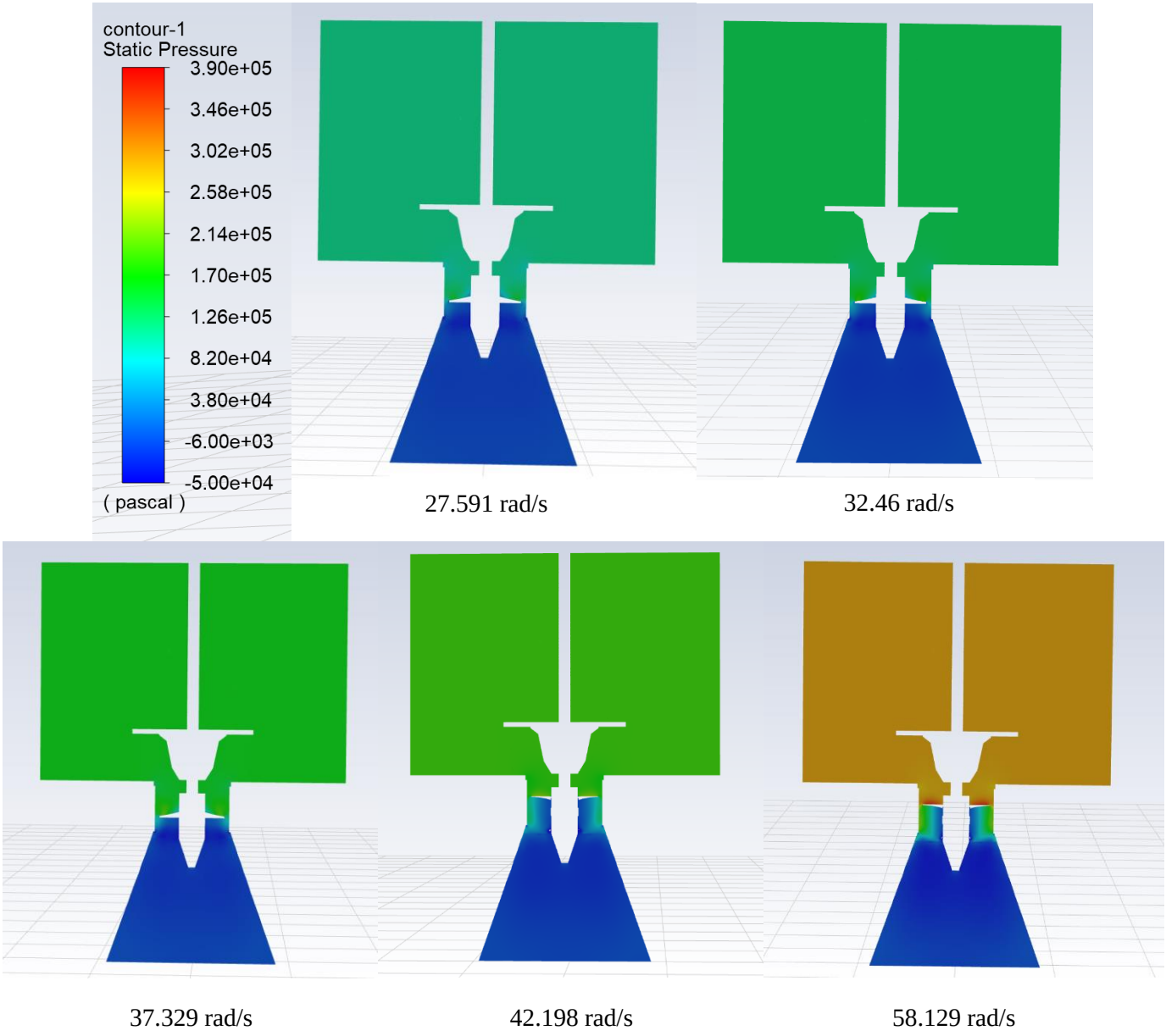

Figure 4.2: Pressure Contours

Pressure contours within the inner domain can be seen in Figure 4.3. The pressure is reduced as it passes across the blades.

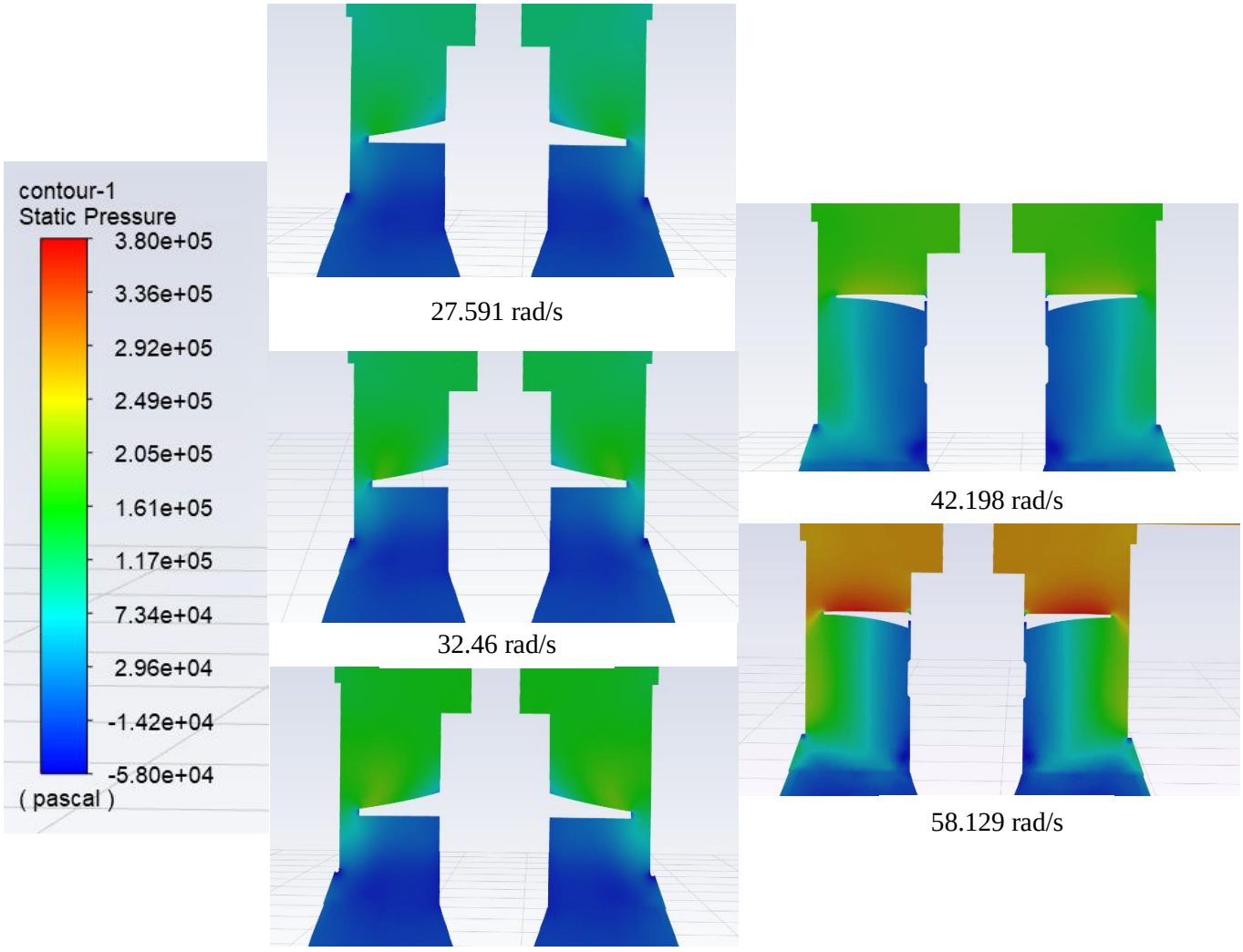

Figure 4.3: Inner Domain Pressure Contours

The velocity contours are given in Figure 4.4. As expected, the velocity magnitude increases while passing over the blades.

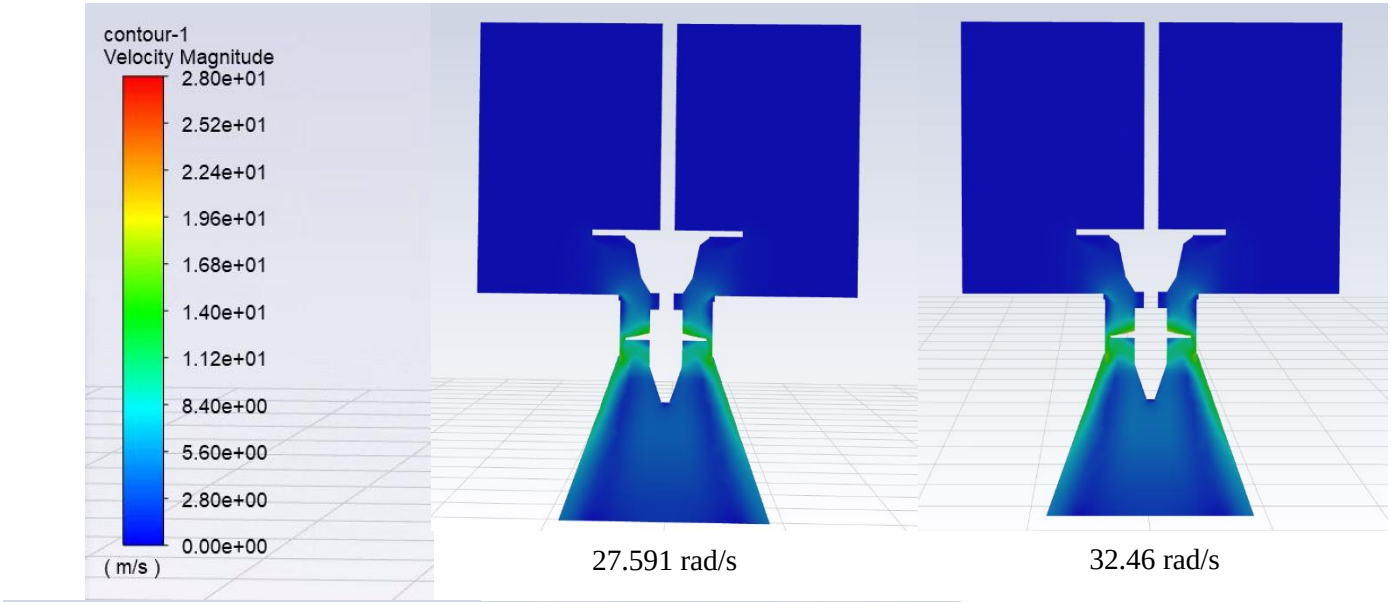

27.591 rad/s

32.46 rad/s

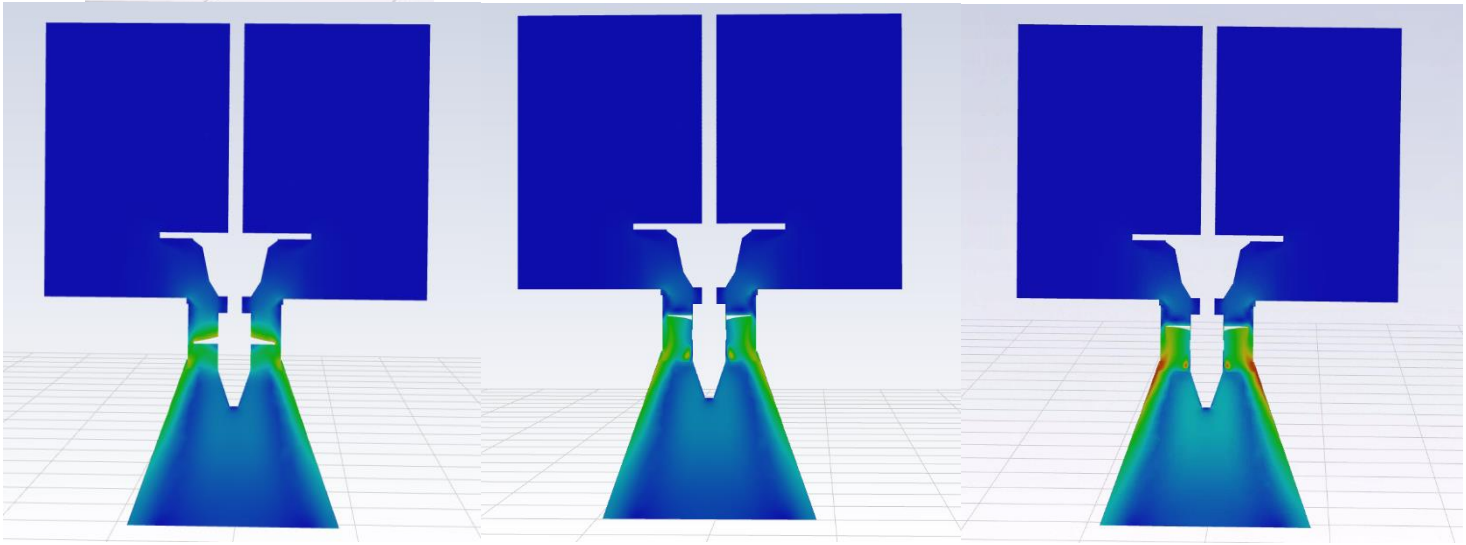

37.329 rad/s

42.198 rad/s

58.129 rad/s

Figure 4.4: Velocity Contours

Another view of the velocity in the inner domain can be seen below in Figure 4.5. The velocity speeds up as it flows over the blades and then slows down significantly as it enters the draft tube.

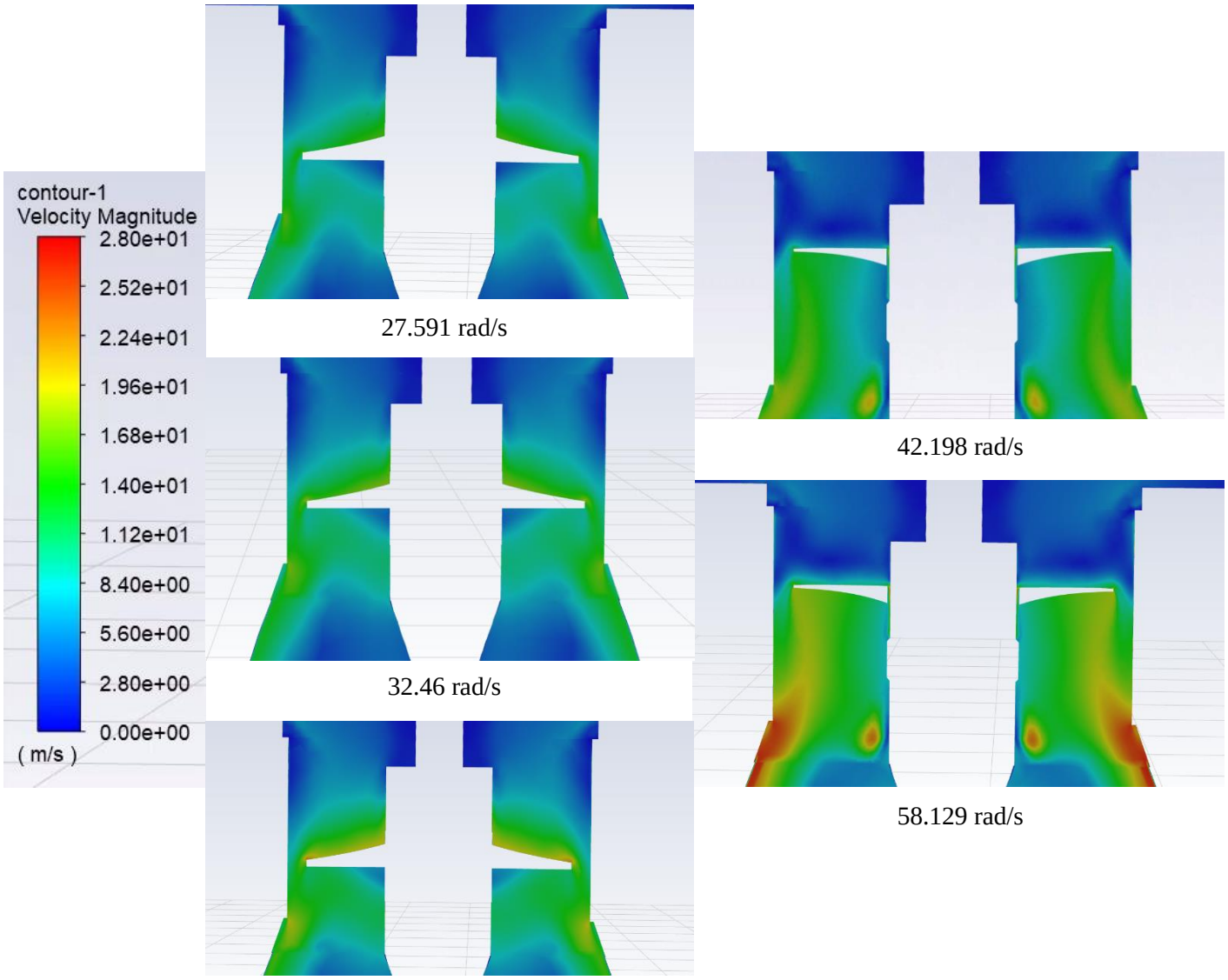

Figure 4.5: Inner Domain Velocity Contours

A cross sectional view of the velocity across one of the rotor blades can be seen in Figure 4.6. As the fluid is passing over the blade, the velocity increases.

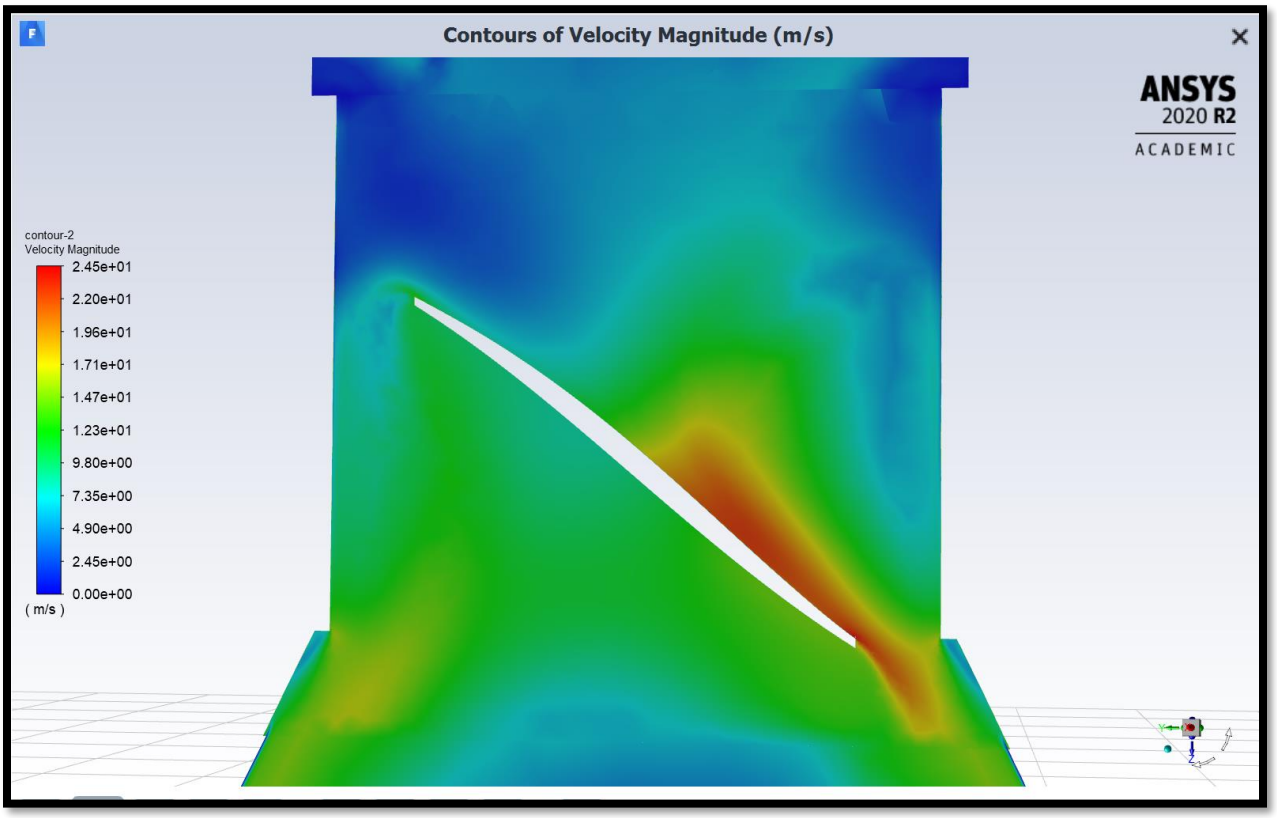

Figure 4.6: Velocity Across Blades at 32.46 rad/s

4.3 Performance Analysis

As discussed in section 3.4, the torque was calculated through this simulation by monitoring the moment coefficient. From the torque, power can be calculated according to equation 3.9.

The computed torque for the 4 cases is shown in Table 4. Due to the increase in rotational velocity, the turbine exerts a higher resistance to the flow with increasing omega. Therefore, the flow field adjusts to a higher inlet pressure, as seen in Figure 4.2. The increase in head leads to an increase in power potential as seen in Figure 4.7 and Table 5.

Table 4: Torque of All Four Cases

Rotational Speed (rad/s)	Torque (Nm)
27.591	2798.45
32.46	3450.31
37.329	4157.06
42.198	4938.32
58.129	7905.00

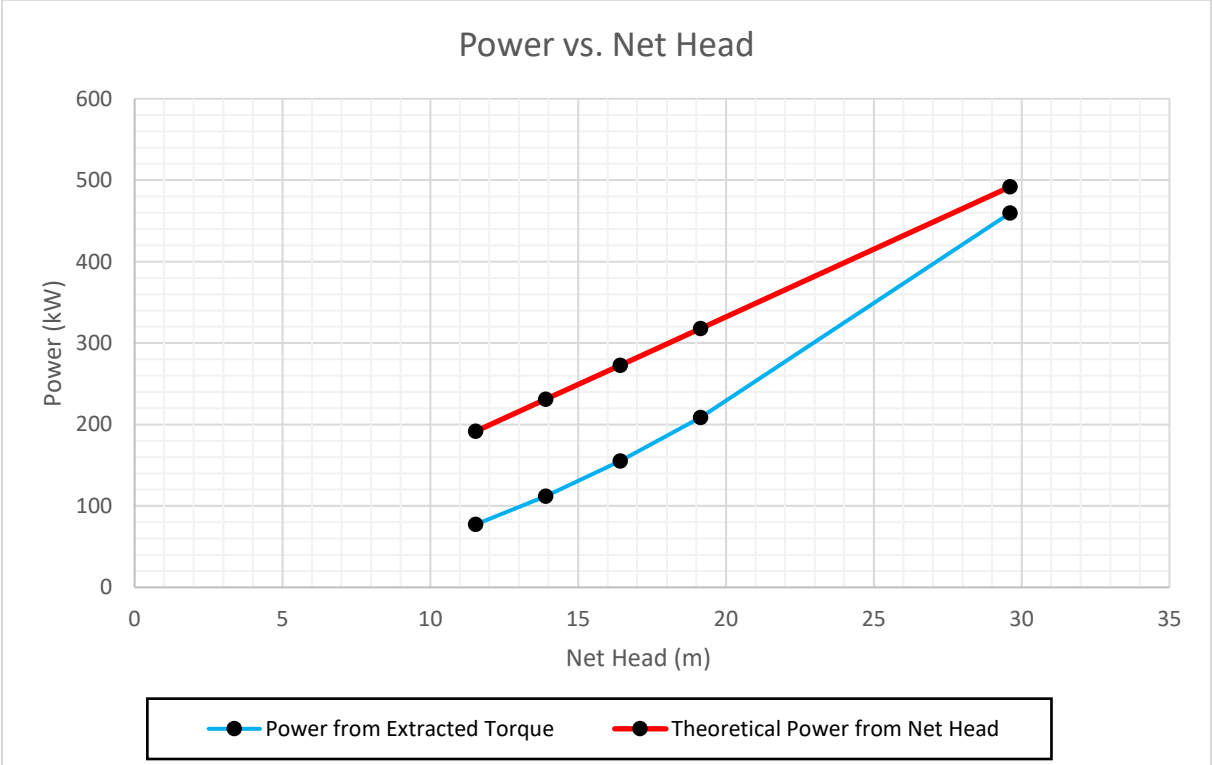

Figure 4.7: Power vs. Net Head

Table 5: Simulated and Theoretical Power Based Off Net Head

Rotational Speed (rad/s)	Net Head [m (ft)]	Power from Extracted Torque (kW)	Power Potential Based Off Net Head (kW)	Efficiency (%)
27.591	11.53 (37.83)	77.21	191.58	40.30
32.46	13.90 (45.60)	112.00	230.91	48.50
37.329	16.42 (53.87)	155.18	272.83	56.88
42.198	19.14 (62.80)	208.39	317.93	65.55
58.129	29.61 (97.15)	459.51	491.76	93.44

As the net head increased, the efficiency also increased. This trend can be seen in Figure 4.8.

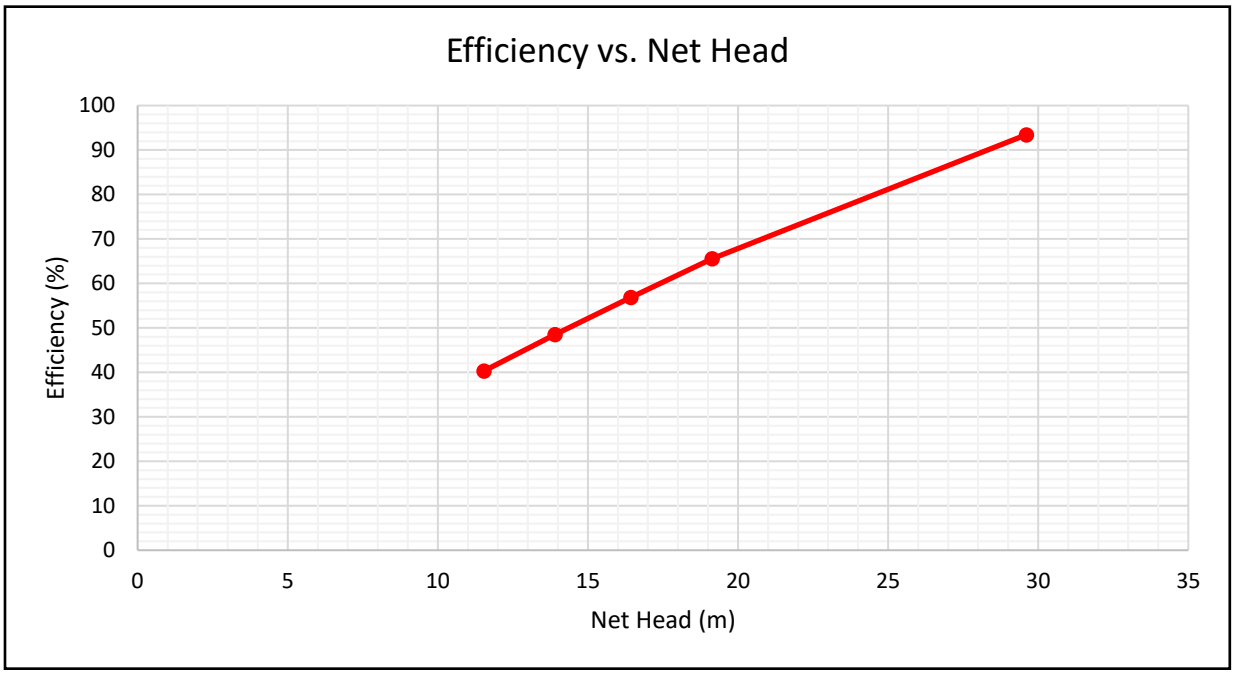

Figure 4.8: Efficiency vs. Net Head

4.4 Experimental Results

To check and validate the results of the simulation, experimental data from Rickly's field sites was obtained. Table 6 shows the values for the flow rate, gross head, power, and other values.

The theta is this table corresponds to the pitch angle of the propeller blades. The gate percentage pertains to the percent the wicket gates are open. Fully open wicket gates (100%) were modeled at 63.127 degrees. From there it is a scalar relationship from 0 to 63.127 degrees for the gate percentage.

Table 6: Experimental Data from Rickly

Case	Flow [m^3/s (cfs)]	Gross Head [m (ft)]	Theoretical Power [kW]	Observed Power [kW]	Theta (degrees)	Gate %	Efficiency
1	0.283 (10)	9.144 (30)	25.42	20	22	20%	0.79
2	1.274 (45)	9.296 (30.5)	116.31	110	22	100%	0.95
3	0.283 (10)	9.144 (30)	25.42	18.5	29	20%	0.73
4	1.614 (57)	9.296 (30.5)	147.33	135	29	100%	0.92
5	1.699 (60)	9.445 (31)	157.63	145	29	100%	0.92

4.5 Validation of Simulation

The closest comparison between experimental case and simulation was case 5 from Table 6 and the slowest rotational speed simulation run which was 27.591 rad/s from Table 5. The rotor blade pitch angle was set at 29 degrees in both situations and the wicket gate opening percentage was at 100%. The flow rate was also taken to be 1.699 $m^3/$ s (60 cfs) in both cases. The rotational speed was not given in the experimental data. The gross head for the experimental case was 9.296 m (30.5 ft) while the net head for the simulation was 11.53 m (37.83 ft).

Net head as discussed earlier is the total energy available to the fluid minus hydraulic losses. The gross head includes these hydraulic losses. Figure 2.1 demonstrates the difference between gross

and net head. As can be seen, the result of the simulation diverges strongly from the experimental results, with efficiencies of 40% for the simulation versus 92% in the field operation. In this thesis, flow rate, rotor blade pitch, and wicket gate angles were kept constant while the rotational speed of the rotor was adjusted which resulted in a change in net head. This contrasts with how the operational space is typically explored for hydro turbines: keeping the head constant and adjusting the flow rate by changing the rotational velocities and/ settings of the gates and blades. Figure 4.9 shows the operating space of a generic Kaplan turbine (Andolfatto). Every blue dot on the figure represents a fixed setting of flow rate, head, rotor pitch angle, and wicket gate setting. The red curves represent the optimal lines of operation for a given head, often also referred to as cam-lines.

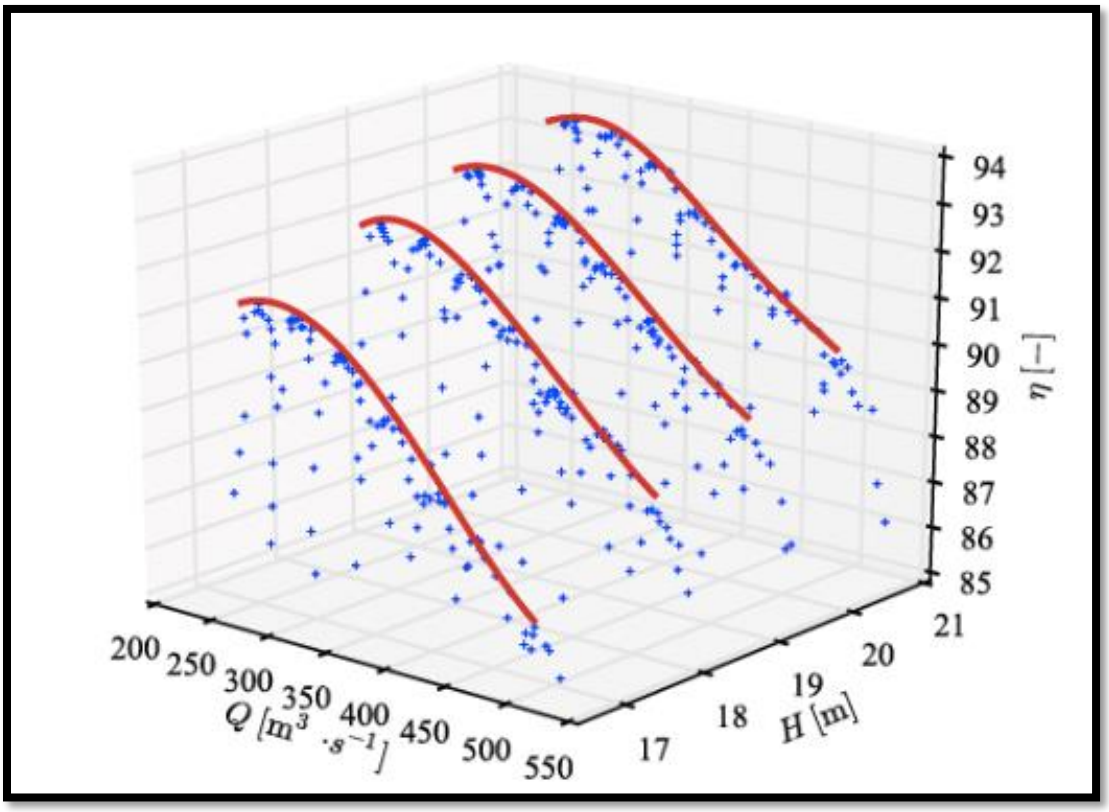

Figure 4.9: Operating Space of a Generic Kaplan Turbine [Andolfatto]

Figure 4.10 shows a 3D plot of the simulation data gathered versus the experimental data obtained from Rickly.

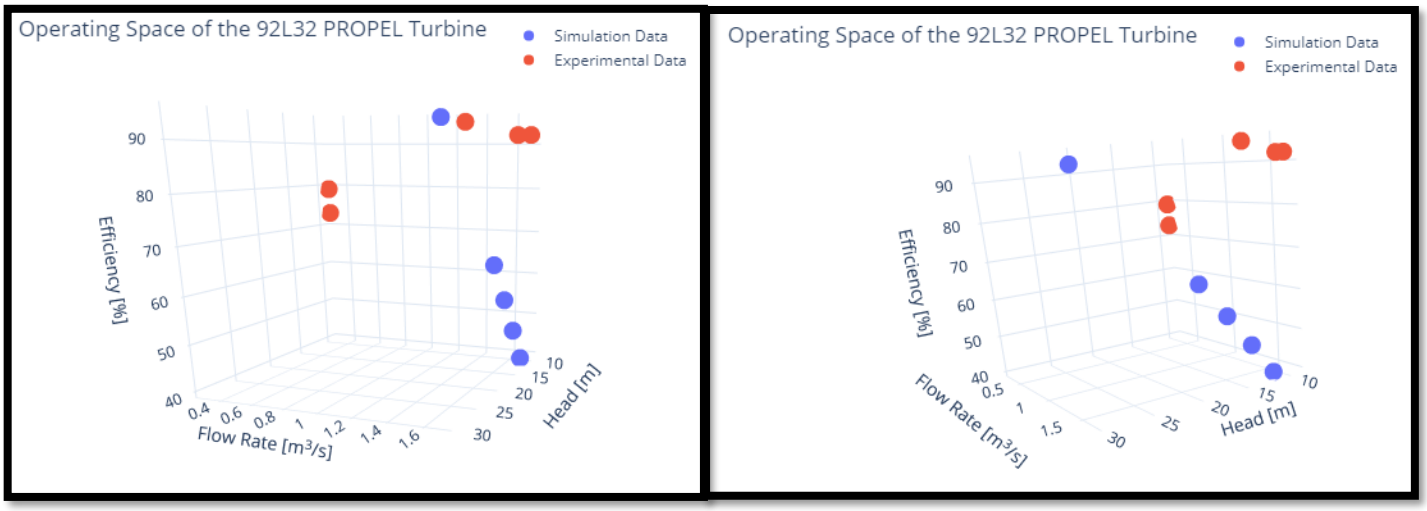

Figure 4.10: 3D Plot of Simulation versus Experimental Data

It should be noted that the experimental data gathered from Rickly uses gross head while the simulation data uses net head. This difference is expected to impact the efficiency prediction of the simulation, leading to higher efficiencies for the simulation (which uses net head) versus the same operating point for the measured data (which uses gross head). . It can also be seen that while the Rickly experimental data stays at a nearly constant head (due to it being collected at one site) and varies in flow rate, the simulation data stays at a constant flow rate and varies in head. In order to better match the experimental data, boundary conditions that can fix the head should be chosen so the head can be fixed and flow rate varied.

5. Conclusion and Future Work

5.1 Conclusions

In conclusion, after five different rotational speeds were simulated, flow fields were generated and analyzed with the intentional of finding the optimal performance point for this turbine. The torque was then calculated from each simulation, and from this, the power was calculated. Due to the increase in rotational speed of the rotor, it was found that the inlet pressure and therefore the net head was increased. This also leads to an increase in power potential. Therefore, as the net head increased, so did the efficiency.

5.2 Future Work

In the future, more work could be performed on this thesis to both further and improve the work found in this paper.

In the future, higher rotational speeds, and therefore higher net heads, could be tested to find the optimal head for 1.699 m^3/s (60 cfs). Also, the head could be fixed by changing boundary conditions and different flow rates could be tested.

Another path for future work on this CFD model would be to manipulate the geometry of this turbine to see how it affects performance. In particular, the propeller and wicket gate angles could be adjusted at different flow rates to see what the optimal combination of angles are for each flow rate.

Bibliography

Andolfatto, Loic, et al. "Automated Hill Chart Modeling to Estimate the Performance of Double-Regulated Units." *Laboratory for Hydraulic Machines*.

Angulo, Mauricio; Liscia, Sergio. 2013. *CFD Optimization of Low Head Turbines Intake Using Fisher-Franke Guidelines.* (October)

ANSYS Inc. (2016), `ANSYS FLUENT 17.2 Theory Guide'.

Breeze P. 2018. Hydropower Turbines. Hydropower.:35–46. doi:10.1016/b978-0-12-812906-7.00004-1.

Cengel, Yunus A., et al. *Fundamentals and Applications of Renewable Energy*.

Clark, Abigail M. *Computational Analysis of Nozzle Designs for a Novel Low Head Turbine*. 2020. The Ohio State University, MS thesis.

Chung, Jaikeun. *Numerical Modeling and Analysis of a Hydrokinetic Turbine in a Confined Geometry*. 2019. The Ohio State University, MS thesis.

Ryan A. Cook. 2017. Final Report of the PROPEL Hydro System. (May).

EIA. 2019. What is U.S. electricity generation by energy source? Available from https://www.eia.gov/tools/faqs/faq.php?id=427&t=3.

Energy.gov. 2014. Hydropower Resource Assessment and Characterization. Available from https://www.energy.gov/eere/water/hydropower-resource-assessment-and-characterization.

Hodge T. 2019. EIA forecasts renewables will be fastest growing source of electricity generation. https://www.eia.gov/todayinenergy/detail.php?id=38053.

Laouari, A., and A. Ghenaiet. "CFD Numerical Simulation of Cavitating Turbulent Flow in a Francis Turbine." *CFD & Tech*, May 2016.

Li, Yunzhue, and Qilin Liu. "Analysis of Hydraulic Performance for Kaplan Turbine Components Based on CFD Simulation." *Earth Environment*, vol. 510, no. 022038, 2020.

Malkus, Thomas. *Computational Analysis of a Novel Turbine Design for Low Head Hydro Power*. 2019. The Ohio State University, BS dissertation.

Munson, B. *Fundamentals of Fluid Mechanics.* 7th ed, John Wiley and Sons, 2012

Rickly. 2020. Rickly PROPEL-Turbine. Available from https://www.ricklyhydro.com/propel-turbine.

Soni, Vishal; Patel Kiran. 2011. *Evaluation of Tubular type Kaplan Turbine*. (December)

Soni, Vishal; Patel, Kiran. 2012. *Evaluation of Vertical Kaplan Turbine using CFD.* (December)

Appendix A

Example Script File:

```
#!/bin/bash
#SBATCH --job-name=parallel_fluent
#SBATCH --time=60:00:00
#SBATCH --nodes=2 --ntasks-per-node=14
#SBATCH -L ansys@osc:1,ansyspar@osc:40
set echo on
hostname
#
# The following lines set up the FLUENT environment
#
module load ansys
#
# Create the config file for socket communication library
#
# Create list of nodes to launch job on
rm -f pnodes
cat  $PBS_NODEFILE | sort > pnodes
export ncpus=`cat pnodes | wc -l`
#
#   Run fluent
fluent 3ddp -t$ncpus -pinfiniband.ofed -cnf=pnodes -g < journal.jou
```

Example Journal File:

```
file/read-case Run33_5000.cas
file/read-data Run33_5000.dat


solve/set/time-step
0.000580645161290323
solve/dual-time-iterate
5000
15

file/write-case-data Run33_5000_POST

exit
ok
```